Laboratori Nazionali di Frascati

To be submited to Il Nuovo Cimento

LNF-89/060(P)
20 Settembre 1989

D. Babusci, L. Casano, A. D'Angelo, P. Picozza, C. Schaerf, B. Girolami:

PROJECT GRAAL: THE SCIENTIFIC CASE

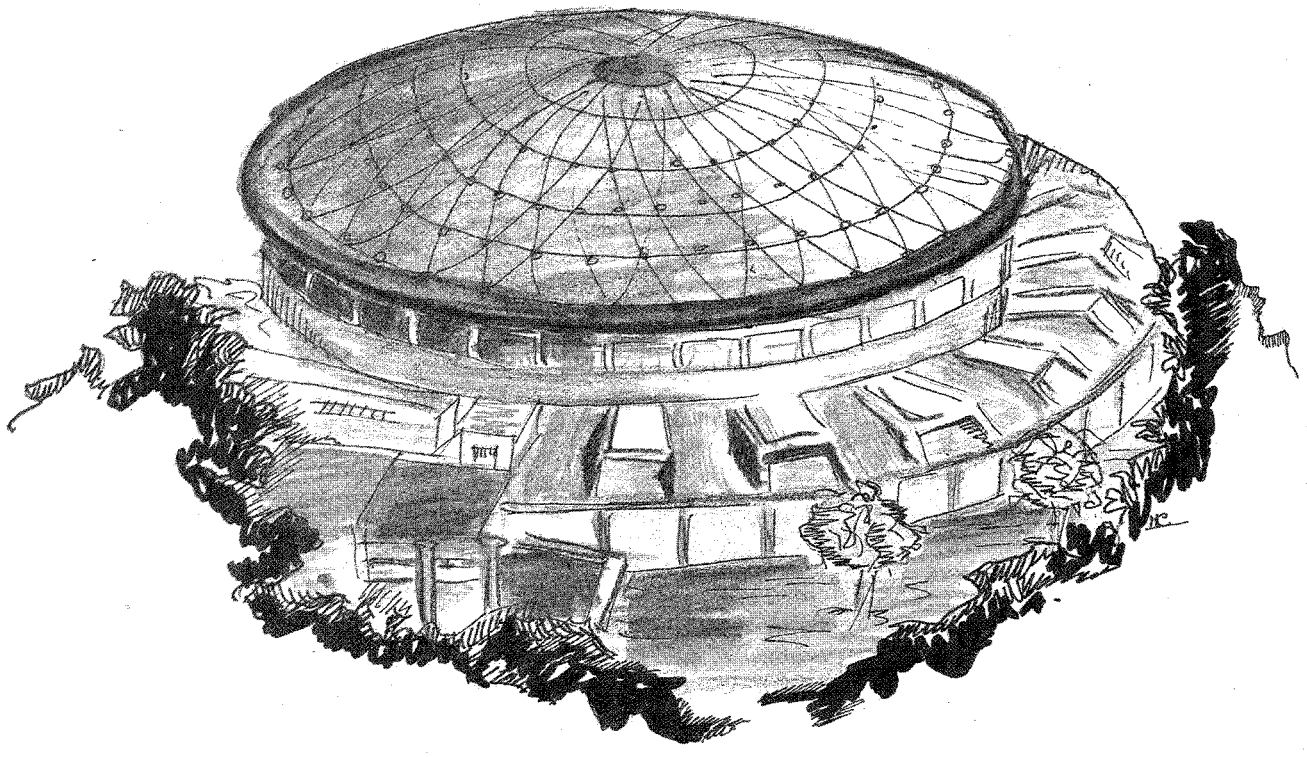

Servizio Documentazione
dei Laboratori Nazionali di Frascati
P.O. Box, 13 - 00044 Frascati (Italy)

INFN - Laboratori Nazionali di Frascati
Servizio Documentazione

LNF-89/060(P)
20 Settembre 1989

PROJECT GRAAL: THE SCIENTIFIC CASE

D. Babusci
INFN - Laboratori Nazionali di Frascati, P.O. Box 13, I-00044 Frascati (Italy)

L. Casano, A. D'Angelo, P. Picozza, and C. Schaerf
Dipartimento di Fisica, Università di Roma , Tor Vergata and INFN- Sezione di Roma - Tor Vergata, Via E. Carnevale, 00173 Roma (Italy)

B. Girolami
Istituto Superiore di Sanità INFN, Sezione Sanità , Via Regina Elena, 00185 Roma (Italy)

ABSTRACT

Backward Compton scattering of Laser light against the high energy electrons circulating in storage rings has produced tagged beams of fully polarized high energy gamma rays with an intensity useful for the study of photoreactions. At the ESRF this technique will produce a beam of 1.5 GeV and an intensity of 10^7 photons sec^{-1}. We discuss the technical characteristics of such a project and the scientific goals which can be achieved in the study of the electromagnetic transitions of the Hadrons and the photoproduction of isobars and strange particles in nucleons and nuclei.

1. INTRODUCTION

The backscattering of Laser light against the 6 GeV electrons circulating in the ESRF will produce a fully polarized gamma-ray beam with a maximum energy of 1.5 GeV. The low emittance of this storage ring will allow tagging the beam with an energy resolution of approximately 1%. The intensity over the entire spectrum should be 10^6-10^7 photons per second depending on the Laser power and the electron current. A useful flux of 10^7 photons/second corresponds to a beam life-time of 47 hours, a value comparable with that estimated for some

insertion devices and much longer than that (10 hours) expected for the entire machine.

The electromagnetic probe has been, for the last half century, a very powerful tool for the study of nuclear and nucleon structure mainly for two reasons:

1) the interaction of the electromagnetic current with particles is well-known and can be treated perturbatively at several levels;
2) the weakness of the electromagnetic coupling constant ($\alpha = 1/137$) allows real and virtual photons to penetrate the nucleus and explore inside its hard core.

Moreover the spatial resolution of 1.5 GeV photons can be understood from Table I:

TABLE I

Average nuclear radius: $R=r_0 A^{1/3}$	$r_0 = 1.2$	fm
Radius of the proton (rms)	$r_p = 0.8$	fm
Wave-length of the photon: h/p_γ	$\lambda = 0.83$	fm
Minimum distance which can be resolved: $\hbar/p_\gamma$	$\delta x = 0.13$	fm

With this resolving power it should be possible to explore well inside the nucleus and the nucleon.

The literature[1] produced in recent years, in part to support proposals for new electron accelerators, contains extensive discussions of the physics which can be done with high energy gamma-ray beams. Therefore we will limit our attention to those cases where photon polarization is essential, emphasizing the fact that the Ladon technique not only produces fully polarized beams, but also allows changing the beam polarization easily and rapidly (by simply changing the polarization of the Laser light), making the measurements of the polarization asymmetries free of systematic errors. For this same reason we have organized our considerations according to the fact that we use linear or circular polarization.

The electric (and magnetic) vector of linearly polarized gamma rays points in a definite direction in the Laboratory System and the electrostatic force acting on the charges, pointing in the same direction, introduces in the azimuthal angle φ easily measurable anisotropies which are very sensitive to the different multipoles contributing to the transition.

Circularly polarized gamma rays correspond to eigenstates of the photon helicity: the photon spin is either parallel or antiparallel to the direction of motion:

$$\vec{s} = \pm \hat{k}$$

This allows the definition of new observables which could be more selective to different reaction mechanisms.

2. COMPTON SCATTERING IN FLIGHT

2.1 Historical background

The fact that backward Compton scattering of Laser light against high energy electrons could produce gamma rays of much higher energy was originally pointed out in 1963 [2] and later demonstrated experimentally by various authors [3].

Subsequently [4] it was pointed out that the high average current circulating in a storage ring coupled with the higher power available inside a Laser cavity could produce a gamma-ray beam with an intensity useful for photonuclear research. This has been experimentally demonstrated at Frascati on the storage ring Adone [5], where a Ladon beam with a maximum energy of 80 MeV has been in use for several years.

The Frascati results have encouraged further speculation and activity, and a beam with a maximum energy of 300 MeV is now entering into operation at Brookhaven National Laboratory [6] on the X-ray machine of the National Synchrotron Light Source (NSLS).

Early studies for a European Synchrotron Radiation Facility (ESRF) immediately suggested[7] the suitability of this machine (due to its high energy and low emittance) for such a facility [8] and a proposal in this direction has been presented in all ESRF books (blue, green and red) [9].

2.2 Kinematics.

The maximum energy of the gamma ray back-scattered by a high energy electron can be put in a simple form in the extreme relativistic approximation (E » m):

$$k_M = E \frac{z}{1+z} \qquad (1)$$

where

E is the energy of the incoming electron,
k_1 is the energy of the incoming photon,
$z = 4 E k_1/m^2$
$\gamma = E/m \gg 1$

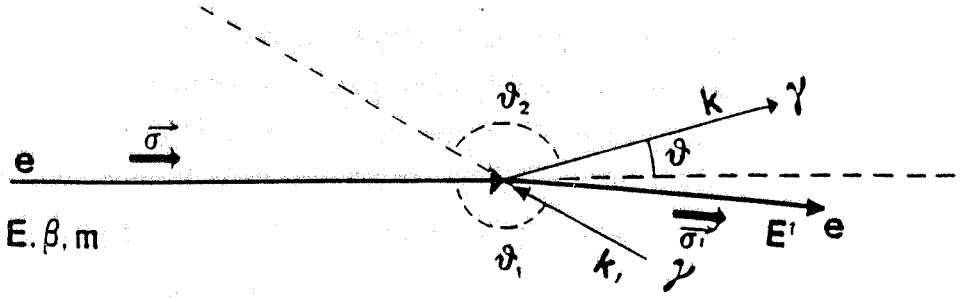

FIG. 1 - Kinematics of the reaction $\gamma + e \rightarrow \gamma' + e'$ in flight.

The energy of photons emitted at a very small angle with the electron direction ($\theta \ll 1$) is given, with respect to k_M, by:

$$\frac{\Delta k}{k_M} = \frac{k_M - k}{k_M} = \frac{x}{1+z+x} \qquad (2)$$

where

$$x = (\gamma \cdot \theta)^2.$$

If $\Delta\theta$ is the semi-aperture of our collimator, then

$$x = (\gamma \cdot \Delta\theta)^2$$

gives some information on the energy band-width of the beam accepted by our collimator.

The angular divergence of the electron beam (σ'_x in the radial plane) sets a lower limit on the angle between the incoming electron and the outgoing gamma ray, and therefore limits the smallest angle of collimation which can be sensibly used and the best monochromaticity obtainable. If

$$x \ll 1 \qquad (3)$$

and

$$z \ll 1$$

then

$$\frac{\Delta k}{k_M} \approx x = (\gamma \cdot \Delta\theta)^2 \approx (\gamma \cdot \sigma'_x)^2$$

2.3 Tagging

Since condition (3) is usually not satisfied at electron energies above 1 GeV, at higher energies we must tag the scattered electron to determine the gamma-ray energy:

$$k = E - E' + k_1 \approx E - E'$$

and

$$\sigma_k^2 = \sigma_E^2 + \sigma_{E'}^2$$

where σ_E and $\sigma_{E'}$ are correlated if we work in a dispersive section.

Two types of tagging have been built: internal and external.

In internal tagging the scattered electrons are momentum analysed by the magnets and quadrupoles of the storage ring. The tagging counters must be located very close to the main orbit of the storage ring and must therefore be remotely removed during injection for two reasons: to free the entire vacuum chamber for the injected electrons and to protect them from the radiation damage of stray electrons.

In external tagging the scattered electrons are removed from the machine lattice with the help of an auxiliary magnetic field located after the first dipole, and are momentum analysed by an external magnetic spectrometer. The auxiliary magnet must be trimmed very carefully to produce a field of less than one Gauss on the main orbit in order not to disturb the circulating electrons.

The calculated performances of both systems are comparable with respect to the gamma-ray

energy resolution (the most important parameter), in the sense that both can reach the limit imposed by the electron beam properties.

Their main differences are:

1) internal tagging is less expensive to build and operate because it does not require new magnets and does not increase the volume of the vacuum chamber by an appreciable amount;
2) since a detector can be located closer to the main orbit than a magnetic field can, internal tagging sets a lower limit on the minimum gamma-ray energy that can be tagged and therefore yields, ceteris paribus, a higher gamma-ray intensity;
3) in internal tagging the detectors must have a high spatial resolution ($\delta x < 1$ mm) and must therefore be Microstrip solid state Silicon Detectors (μSD) or scintillating optical fibers. Being very close to the beam they will suffer radiation damage and will have to be replaced periodically:
4) in external tagging the detectors do not need a very high spatial resolution ($\delta x \approx 10$ mm) and can therefore be made out of more stable plastic scintillators. They can be located at a reasonable distance from the ring in a radiation-safe location which could be accessible with the ring in operation.

The energy resolution of an internally tagged Ladon beam has been derived by M. Preger [8] in the linear approximation:

$$\sigma_k = E\,\sigma_{xT} / d$$

where

$$\sigma_{xT}^2 = \varepsilon_x \beta_{xT} + \eta_T^2\,\sigma_P^2$$

and

d is the energy dispersion of the magnetic components of the ring lattice from the interaction region to the tagging detectors (A_{13} in many matrix notations) [m];

ε_x is the horizontal emittance of the stored beam [m·r];

σ_P is the fractional energy spread of the stored beam;

β_{xT} is the horizontal betatron wave-length at the position of the tagging detectors [m];

η_T is the energy dispersion at the position of the tagging detectors [m];

ε_x and σ_P are global machine parameters, β_{xT} and η_T depend on the position of the tagging detectors, while d depends on the positions of the interaction region and the tagging detectors.

The purpose of our calculations has been to determine these two positions in order to minimize the value of σ_k.

3. THE CASE OF THE ESRF

3.1 Photon spectrum and energy resolution.

Numerical results for the ESRF were originally obtained by M. Preger et al. [8] and recently repeated by two of us (D.B, L.C.) using a Monte Carlo simulation. They followed the

trajectories of the scattered electrons in the storage ring magnetic lattice from the interaction region to the position of the tagging detector conveniently located in the storage ring where the energy resolution is close to its best value. Our results have also permitted the identification of 0.6 mm as the maximum pitch of the tagging counters which does not appreciably affect the energy resolution.

The basic cell of the ESRF (1/32 of the storage ring) consists of two dipoles separated by four quadrupoles as indicated in Fig. 2. The distance between the two dipoles is 6.4 m and at the far end of each dipole there are three quadrupoles and a magnetic-field-free region devoted to insertion devices like Wigglers or Undulators. Therefore, between the dipoles, the machine alternates one short straight section (6.4 m) and a long one (14.1 m). The long straight sections are dispersion-free and at their center can have a low β for insertion of a Wiggler or a high β for insertion of an Undulator. We will call them respectively W sections and U sections. The short straight sections have in their center a dispersion of approximately O.5 m and therefore we will call them D sections.

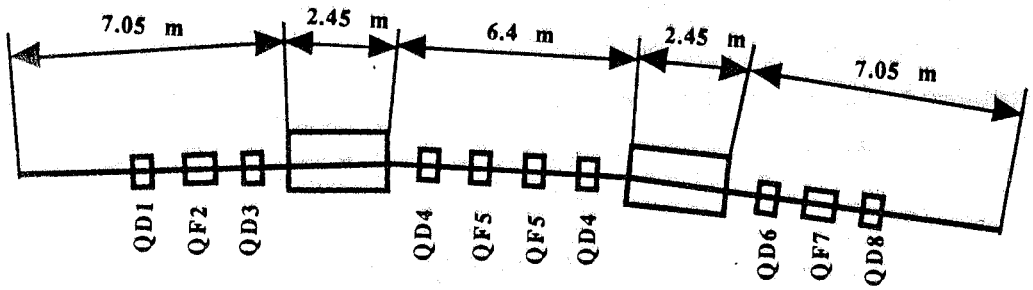

FIG. 2 - The basic celle of the ESRF. 1/32 of the storage ring.

Since the Laser electron interaction shall take place in a straight section we have four possible alternatives for the position of the interaction and tagging regions:

Interaction region	Tagging region (μSD)
D	W
D	U
W	D
U	D

Since the angle of scattering of the electrons in the Laboratory is very small and lower than the angular divergence of the electron beam, electrons of different energies move in the same way in the quadrupoles located before the first bending magnet. Therefore the last two solutions are very similar and we can study only one of them.

If we now suppose that the interaction region is located in a dispersion-free section like U or W ($\eta_I = 0$), then the dispersion from the interaction region to the μSD is similar to the dispersion

of the machine:

$$d = \eta_T$$

and

$$\sigma_{xT} \geq \eta_T \sigma_P$$
$$\sigma_k \geq \sigma_E$$

where

$$\sigma_E = E\,\sigma_P$$

The energy resolution in MeV of the gamma-ray beam is at best the same as that of the primary electron beam. The magnetic lattice does not operate as an energy loss spectrometer with respect to the energy lost by the electron to the photon during the scattering process.

Only in a dispersive region we can have a correlation between the energy of the initial and final electrons with some improvement in the gamma-ray energy resolution. For this reason we have found empirically that the energy resolution is better if we place the interaction region in a D section and the μSD in the following U or W section where η is zero. In this way the γ ray energy resolution is given by:

$$\sigma_k = \frac{E}{d}\sqrt{\varepsilon_x \beta_{xT}} = E\sqrt{\varepsilon_x}\ \frac{\sqrt{\beta_{xT}}}{d}$$

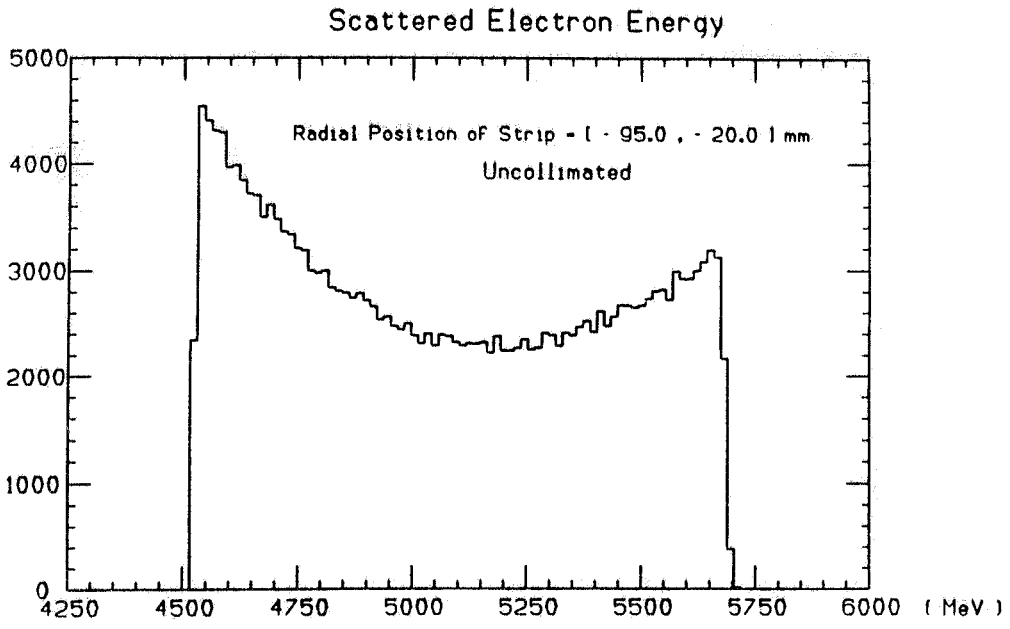

FIG. 3 - The energy distribution of scattered electrons detected by our tagging counters. The microstrips cover a radial displacement from 20 mm to 95 mm from the equilibrium orbit.

The Monte Carlo results which follow assume the μSD in a W section at the entrance to a QF7 focusing quadrupole, but the results for a U section are comparable.

The spatial distribution of the electrons has been calculated from the numbers in the red book. For the Laser we have assumed a gaussian beam having a waist with a radius of 0.3 mm (rms) in the center of the straight section.

The energy distribution of the scattered electrons is indicated in Fig. 3. We have assumed that the tagging counters start 20 mm from the circulating electron beam and extend for 75 mm to detect the electrons which have lost maximum energy. Fig. 4, curve (a), represents the uncollimated distribution of the tagged gamma rays as they exit the accelerator. Their polarization is indicated in Fig. 5. The intensity through a collimator with a diameter of 10 mm placed 25 m from the center of the interaction region is represented by curve (b) in Fig. 4. This is a useful distance for small experiments which do not need too much space in the experimental hall. For larger experiments we have assumed the same collimator placed at 50 m distance.

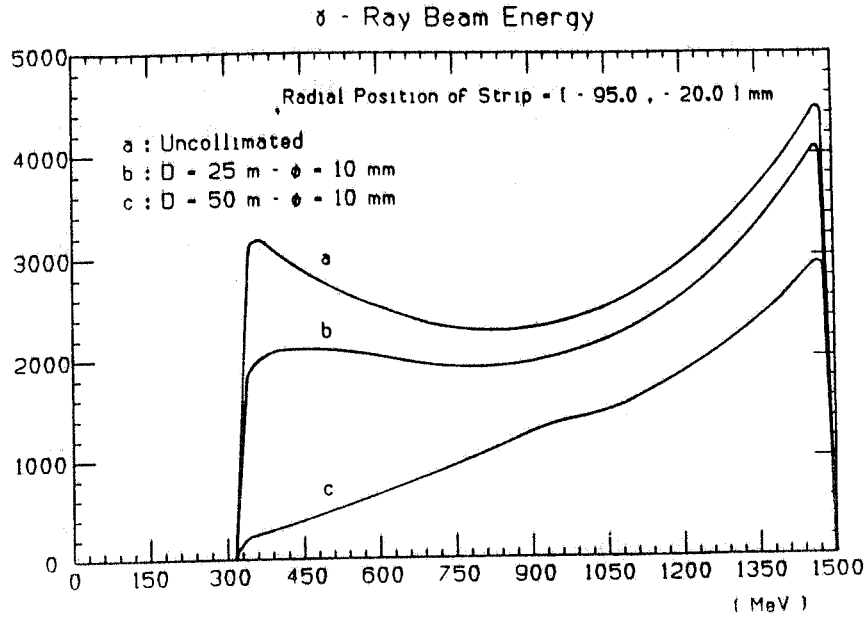

FIG. 4 - a) the uncollimated energy distribution of tagged gamma rays as they exit the storage ring; b) the energy distribution of tagged gamma rays passing through a collimator with a diameter of 10 mm located 25 m from the center of the interaction region; c) as above with the same collimator situated at 50 m.

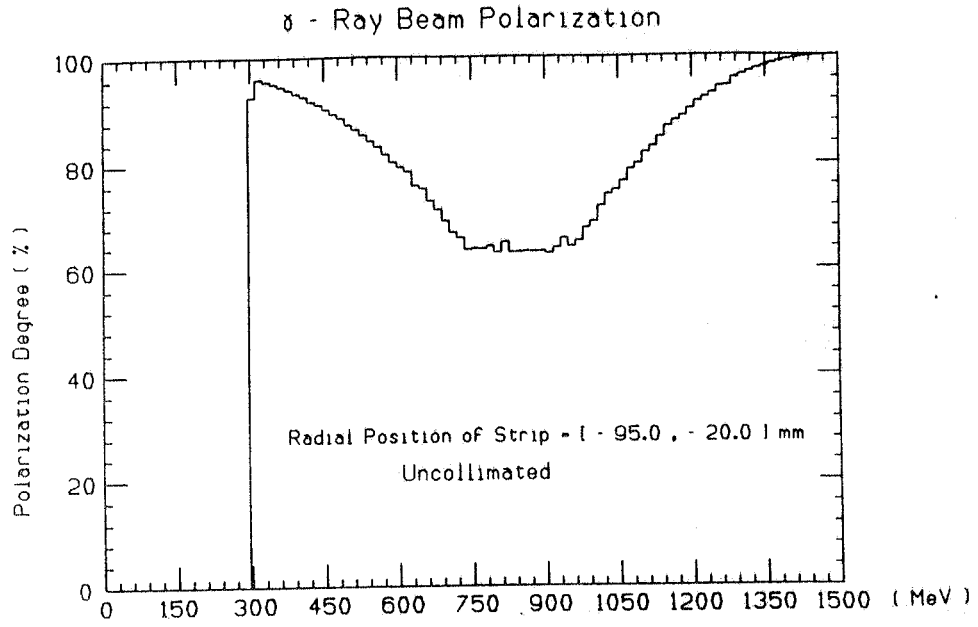

FIG. 5 - The polarization of the uncollimated tagged gamma-ray beam

The respective spectrum is the lowest curve (c) in Fig.4. Comparing these three curves we observe that moving our collimator further from the ring drastically decreases the intensity of gamma rays at low energies while at high energy the reduction is of the order of only 25%. Good news for those interested in the photoproduction of strange particles. Fig.6 represents the spectrum of gamma rays in coincidence with one channel of the tagging counters. At a gamma-ray energy of 1400 MeV it gives a resolution of 18 MeV (FWHM) or 1.3%. This very encouraging result is the consequence of the low emittance of the ESRF. In its energy range it is the only storage ring, now under construction, with such a small value of ε_x.

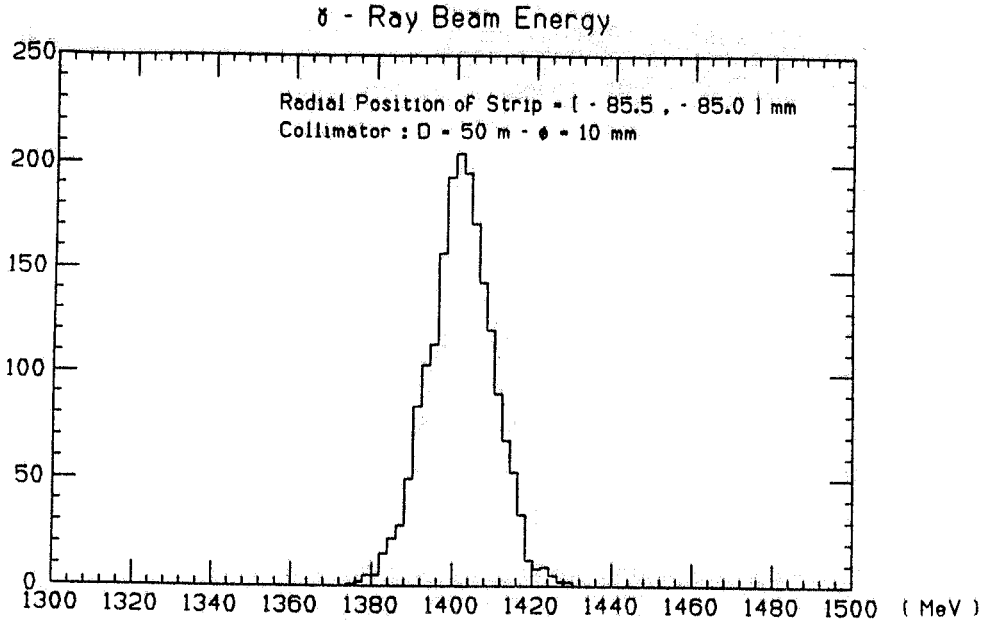

FIG. 6 - The spectrum of gamma-rays in coincidence with one channel of the tagging spectrometer.

3.2 Luminosity, intensity and beam mean life.

The total gamma-ray beam intensity is given by the cross section multiplied by 2 c (the relative velocities of electrons and photons in the Laboratory System) and the convolution of the Laser and electron spatial densities:

$$\frac{dn}{d\Omega} = 2c \frac{d\sigma}{d\Omega} \int u_1 u_2 \, dV$$

$$n = 2c \; \sigma \int u_1 u_2 \, dV = P I L.$$

where:

P is the Laser power in Watt

I is the electron current in Ampere

L is the luminosity in $s^{-1}W^{-1}A^{-1} = W^{-1}Q^{-1}$

As we have already anticipated the Laser spatial density distribution has been assumed to be

Gaussian with a waist in the center of the straight section of the order of 0.3 mm (rms). On the other side the spatial distribution of the electrons is Gaussian in the coordinates orthogonal to the beam direction with the variances σ_x and σ_z given by the the values of ε_x, ε_z and indicated in Fig. 1.3.4 of the red book[9b]. Since the dominant σ_x has a maximum in the center of the straight section, the electron density has a minimum where the Laser density has its maximum. Therefore the production of gamma rays is not much different over the entire length of the interaction region. The final integration has been performed numerically with the result:

$$L = 2.6 \cdot 10^7 \ s^{-1}A^{-1}W^{-1}$$

Since almost all the scattered electrons are removed from the circulating beam the number of electrons lost per second $(\dot{N}_e)$ is equal to that of the gamma rays produced:

$$\dot{N}_e = n_\gamma = L\,P\,I = L\,P\,N_e\,e\,/T = N_e\,L\,P\,e\,/T = N_e/\tau$$

where:

$$\tau = T/L\,P\,e$$

is the <u>beam mean life</u> produced by the operation of the Laser,

e is the electron charge and

T is the revolution period in the ESRF (2.8 μs).

With a Laser power of 4 W, now commercially available, we have:

$$\tau = 2.8 \cdot 10^{-6}/\ 2.6 \cdot 10^7 \cdot 4 \cdot 1.6 \cdot 10^{-19} = 1.7 \cdot 10^5 \text{ s} = 47 \text{ hours}$$

Which corresponds to a tagged and collimated intensity:

$$N = 1.1 \cdot 10^7 \ s^{-1}$$

In Table II we have indicated the different Ladon beams now in operation, under construction or being planned.

TABLE II

Project name	Ladon°	Taladon+	Legs*	Graal**
Location	Frascati		Brookhaven	Grenoble
Energy defining method	collimation	internal tagging	external tagging	internal tagging
Electron energy GeV	1.5		2.5	6
Photon energy eV	2.45		3.53	3.53
Gamma energy MeV	5-80 variable	35-80 simultaneous	180-300	300-1500
Energy resolution FWHM				
MeV	0.07-8	4-2	6	18
%	1.4-10	5	2	1.2
Electron current A	0.1		0.2	0.1
Gamma intensity s^{-1}	10^5	$5 \cdot 10^5$	10^7	10^7
Date of operation (expected)	1978	1989	1987	1995

° Laser **ADONE**, +**TA**gged **LADON**, * Laser Electron Gamma Source, ** **GR**enoble **A**nneau **A**ccelerateur **L**aser.

4. LINEARLY POLARIZED GAMMA RAYS

The angular distributions for the scattering of linearly polarized photons for the first three electromagnetic multipoles (E1, M1 and E2) are represented in Fig. 7 (from B. Ziegler in ref. 1a).

Their striking difference immediately evidences the fact that the use of linearly polarized gamma rays will allow a much better separation of the different multipoles contributing to the transition, with a comparable improvement in our understanding of the reaction mechanism.

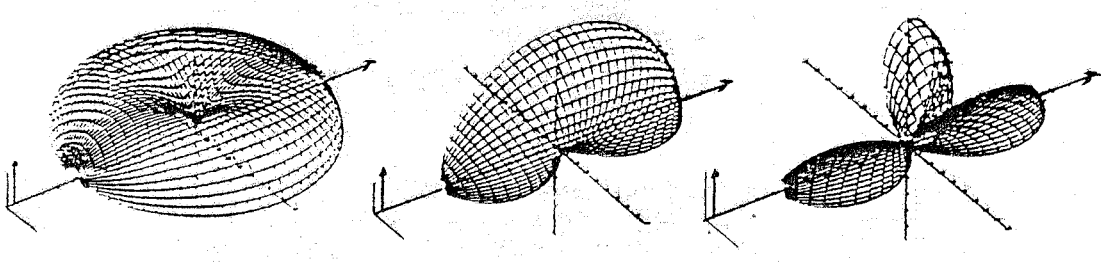

FIG. 7 - The angular distribution for the scattering of a 100% linearly polarized gamma-ray beam from the first three multipoles: E1, M1 and E2. The differential cross section $d\sigma(\theta,\varphi)/d\Omega$ is proportional to the distance of a point of the surface to the origin. The net represents curves with θ=const. and φ=const; step width in both directions is $\pi/36$; θ runs from 0 to π, φ from $-\pi/2$ to $\pi/2$.

4.1 The nucleon

In the energy region made available by this project (300-1500 MeV) the nucleon exhibits all its major resonance states. Fig. 8 from ref. [10] shows the total photoabsorption cross section of the proton.

The contributions of the Δ_{33} (1232), N_{13} (1520) and N_{15} (1680) isobars are clearly manifest from the data. Each of them has a definite spin and parity and can be excited by an electric or a magnetic multipole according to Table III.

TABLE III

Isobar	spectroscopic notation	isospin 2T	spin 2S	parity $P=(-)^l$	allowed transitions
Δ_{33}	P_{33}	3	3	+	M1, E2
N_{13}	D_{13}	1	3	-	E1, M2
N_{15}	F_{15}	1	5	+	M2, E3

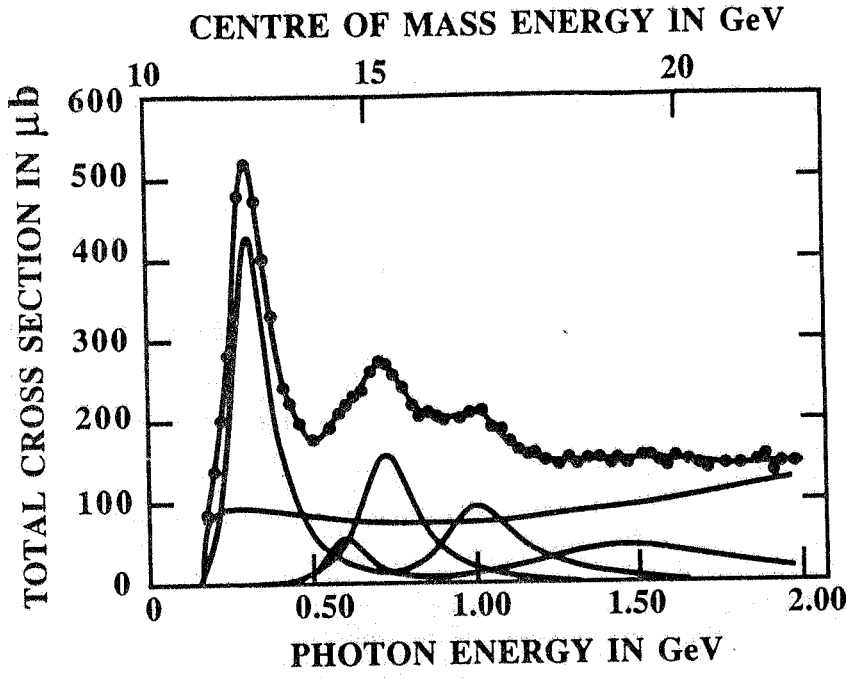

FIG. 8 - The total photoabsorption cross section on the proton: the curves beneath the three peaks show a fit to the resonance cross section corresponding to the M1, E1 and E2 proton excitation respectively. The flat curve is the background; the other curves come from states with lower excitation probability.

The transition mechanisms of the proton to the various resonances are quite different for electric or magnetic multipoles and their investigation constitutes a testing ground of various QCD models. The angular distribution for meson photoproduction corresponds to an explicit function

of θ and φ for the assigned values of the isobar quantum numbers and the multipolarity of the transition. Thus experiments with linearly polarized gamma rays will allow the determination of the relative weight of the electric and magnetic transitions.

To understand the importance of these measurements let us fix our attention on the first isobar: Δ_{33} (1232).

In a simple quark model, the nucleon and the delta resonance belong to the same multiplet, and a transition from one to the other is induced by the spin-flip of a **u** quark stimulated by an M1 multipole

particle (MeV)	Isospin 2T	spin 2S	quark spins
Δ (1232)	3	3	$d\uparrow u\uparrow u\uparrow$
			$\uparrow$ M1
N (938)	1	1	$d\uparrow u\uparrow u\downarrow$

The detection of an E2 transition would require a D-wave component in the three-quark wave function, a suggestion for tensor quark-quark forces in the nucleon and the presence of non spherically symmetric states in the nucleon or the isobar. However the smallness of the E2 contribution has made very difficult to evidence it from the measurements of the differential cross section despite the abundance of available data. For this reason the more discriminating measurements of polarization asymmetries, and their relative immunity from systematic errors, can make the detection of this important but elusive quantity finally possible.

Moreover according to reference 11 we have:

$$E2 = \frac{1}{\sqrt{3}}[A(3/2) - A(1/2)]$$

where A(3/2) and A(1/2) are the helicity amplitudes for the photon-nucleon interaction in the states of spins parallel (J=3/2) and antiparallel (J=1/2) respectively.

There exists now several determinations of the helicity amplitudes and the E2/M1 ratio as indicated in Table IV, taken from ref.11. They all agree on a value between -1.1% and -1.5% with an error of approximately 1%. Only this last paper quotes a much smaller error (0.2%) on the basis of a new analysis of all existing data. Obviously, a new accurate determination with a different experiment is highly desirable.

The nucleon-isobar transition can be studied with photons through three reactions:

$$\gamma + p \rightarrow n + \pi^+$$
$$\gamma + p \rightarrow p + \pi^\circ$$
$$\gamma + p \rightarrow p + \gamma$$

TABLE IV

Observable	MW	CM1	CM2	PDH	MDWBH
A3/2 ($GeV^{1/2}$)	- 245 ± 7	- 247 ± 10	- 263 ± 26	-258 ± 11	-229 ± 6
A1/2 ($GeV^{1/2}$)	- 140 ± 6	- 136 ± 6	- 145 ± 15	-141 ± 5	-125 ± 3
EMR %	- 1.2 ± 1.3	- 1.2 ± 1.5	- 1.1 ± 3.5	-1.4 ± 1.4	-1.5 ± 0.2

In the photoproduction of π^+ the term originating from the direct coupling of the photon to the pion is very large and therefore makes the separation of the resonant amplitudes more difficult. For this reason, we will not discuss the first reaction.

The possibility of extracting the E2/M1 ratio from the resonant Compton scattering of linearly polarized gamma-rays on the proton has been extensively discussed in ref. 12. It is shown that a value of E2/M1 of 1% will produce a change of 2.4% in the difference of the cross-sections for the two directions of polarization and in the value of the asymmetry.

The values of the two cross sections in the two polarization planes can be measured simultaneously using two identical apparatuses. The role of the two apparatuses can be alternated by frequently and randomly rotating the polarization of the Laser light. In this way, we can produce a result that is practically free of systematic errors.

In the asymmetry the statistical error is given by:

$$\Delta\Sigma = \frac{2}{\sqrt{N}}$$

where N is the total number of counts in both directions of polarization.

At 320 MeV the differential cross section at 90° in the CMS has a value of 200 nb/sr. Since not all data taken at all angles are equally effective in determining the asymmetry, we can reasonably assume that the useful statistics is equivalent to that collected in a total solid angle of 1 steradian around the direction of 90° in the CMS and the two polarization planes. With these hypotheses we have:

$$N = N_H N_\gamma \frac{d\sigma}{d\Omega} \Delta\Omega = 4.2 \cdot 10^{23} \; 2 \cdot 10^{6} \; 2 \cdot 10^{-31} = 0.17 \; s^{-1}.$$

where:

N_H = $4.2 \cdot 10^{23}$ is the number of protons in a liquid Hydrogen target 10 cm long;

N_γ = $2 \cdot 10^6$ s^{-1} is the number of photons per second in an energy interval of 100 MeV produced by an Argon Ion Laser with a power of 6 Watt;

$\frac{d\sigma}{d\Omega}$ = 200 nb/sr

$\Delta\Omega$ = 1 sr.

In two months we have:

$$N = 440\,000$$

and:

$$\Delta\Sigma = \frac{2}{\sqrt{440000}} = 3\ 10^{-3}$$

From which:

$$\Delta(E2/M1) = 3\ 10^{-3}\ /2.4 = 1.26\ 10^{-3}$$

This will provide an improvement in accuracy and a test of the value obtained in ref. 11 through a new analysis of all existing photon-proton data.

The uniqueness of the GRAAL facility is the availability of a gamma-ray beam with circular polarization very close to one. The measurement of spin-spin correlations is made easy by the fact that the photon spins can be reversed by simply changing the polarization of the Laser light leaving the more critical target polarization unchanged. Therefore we can assume that the values of the asymmetry are free of systematic errors. The experiment could be easily performed detecting, with the BGO crystal ball, the two gammas emerging from the decay of the π° photoproduced in the Hydrogen nuclei of the target. With a counting rate of tens of counts per second, the limiting factor is not counting statistics, but the fact that the most common present day polarized Hydrogen targets are not made of pure Hydrogen but contain other elements. The polarized target material now more widely used is ammonia (NH3). Unfortunately Nitrogen is a spin 1 nucleus and its degree of polarization in an ammonia target is not very well known. For this reason it is better to use other compounds like Butanol or other alcohols which, beside Hydrogen, are composed of Carbon and Oxigen whose dominant isotopes have spin 0.

Ammonia targets are now more popular than Butanol because they are much more radiation resistant. Fortunately this is not a problem with gamma-ray beams like Graal since their limited intensity does not produce appreciable depolarization.

With a proton polarization around 70% and the possibility of subtracting the contribution of Oxigen and Carbon with independent runs with different targets, the main source of error in our experiment will be the stability and reproducibility of the target polarization. Today we can probably assume an error around 2% but the constant improvements in this technology gives good hopes for the near future.

An error of 2% in the measurements, and a polarization of 70%, will imply an error in the cross sections of about 3% and in the helicity amplitudes an error of 1.5 %. This is an appreciable improvement over the values given in Table IV.

In the energy region covered by this facility (300-1500 MeV) the minimum value of the gamma-proton total cross section is of the order of 150 μb. The integrated yield is therefore given by:

$$n_{\gamma p} = N_o\ N_\gamma\ \sigma_T\ l\ \delta = 6 \cdot 10^{23} \cdot 10^{7} \cdot 150 \cdot 10^{-30} \cdot 5 \cdot 0.07$$

$$n_{\gamma p} \approx 315\ s^{-1}$$

a very comfortable number which should allow the separate measurements of the various reaction

channels including Compton scattering which has a cross section lower by about two orders of magnitude.

4.2 The deuteron.

Detailed theoretical calculations have been performed [13] in the case of deuteron photo-disintegration

$$\gamma + d \rightarrow p + n$$

where a large amount of experimental data is available [14].

They have shown that the standard theory, which has given satisfactory fits to the experimental data of the unpolarized differential cross section, is not adequate to explain the polarization asymmetries even at energies of a few tens of MeV. To explain these data, Meson Exchange Currents (MEC) and Isobar Configurations (IC) must be added explicitly at all energies, well below the pion production threshold. This is clearly indicated in Fig. 9 which indicates, at a center of mass angle of 90°, the asymmetry

$$\frac{d\sigma_{\parallel} - d\sigma_{\perp}}{d\sigma_{\parallel} + d\sigma_{\perp}}$$

where

$d\sigma_{\parallel}$ is the differential cross section in the polarization plane;

$d\sigma_{\perp}$ is the differential cross section in the plane perpendicular to the direction of polarization.

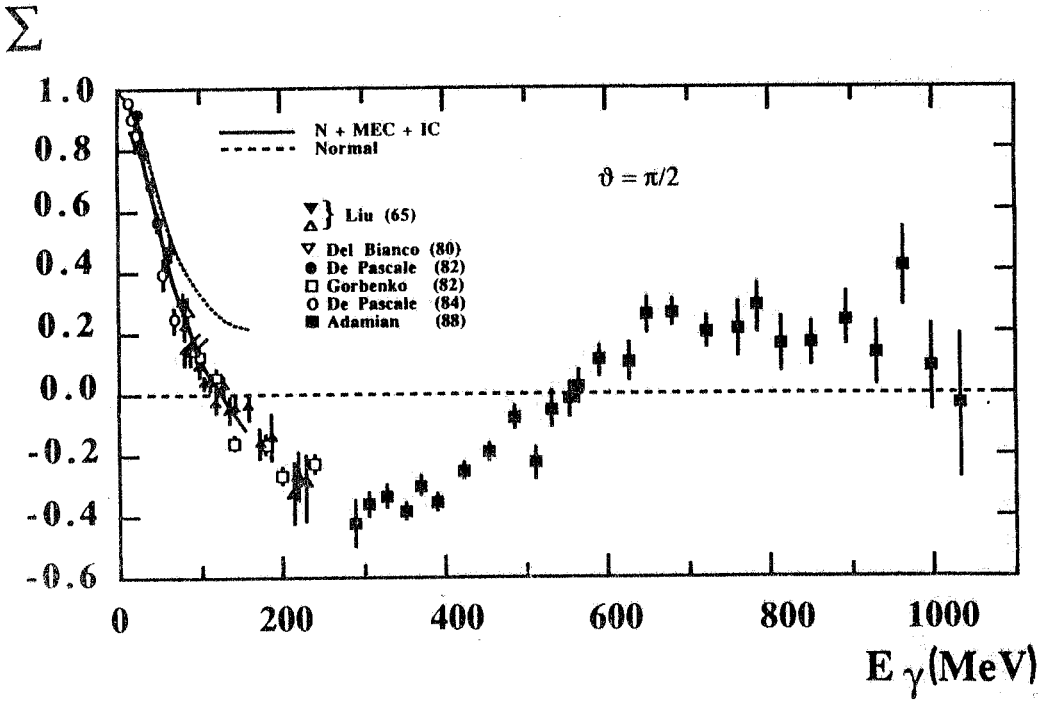

FIG. 9 - The asymmetry for the reaction $\gamma + d \rightarrow p+n$ as a function of gamma-ray energy at CM angle of 90°.

The calculations have now been extended to the case of polarized deuteron targets [15] to show an even greater dependence on the details of the reaction mechanism.
At higher energies the cross section has been calculated [16] from QCD in terms of the basic quark and gluon degrees of freedom, and found to be in reasonable agreement with the existing measurements [17]. The most striking experimental fact is that only the first pion-nucleon resonance (Δ_{33}) appears as a bump in the data. The contributions of the higher resonances are not apparent in the angular distributions. Polarization data might therefore help to understand this phenomenon.

Assuming a value for the total cross section of 0.5 μb at 1 GeV and a liquid deuterium target 5 cm long we have a total photodisintegration rate of 1 per second:

$$n_d = N_o N_\gamma \sigma_T \, I \, \delta/A = 6 \cdot 10^{23} \cdot 10^7 \cdot 0.5 \cdot 10^{-30} \cdot 5.0 \cdot 0.16 / 2 = 1 \ s^{-1}$$

A comfortable rate which will allow the accurate measurements of many asymmetries even with spectrometers of moderate solid angle ($\Delta\Omega \approx 0.1$-1 sr).

4.3 The three-nucleon system.

The results obtained at Frascati in 1972 [18] for the polarization asymmetries of the reaction:

$$\gamma + He^3 \rightarrow p + d$$

have recently been confirmed at Karkhov [19] and extended to different angles and energies (Fig. 10). Theoretical models [20] reproduce the differential cross sections at small angles while large uncertainties still exist at high momentum transfer and for the polarization asymmetries.

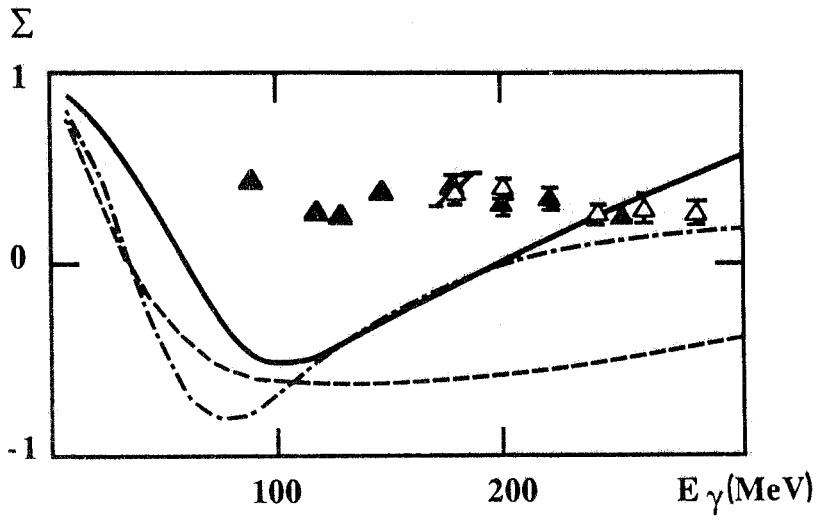

FIG. 10 - The asymmetry for the reaction $\gamma + He^3 \rightarrow d + p$ as a function of gamma-ray energy at a CM angle of 90°. Points Δ and ▲ are taken from refs. (18) and (19). The curves have been calculated in ref. (20b) using the RSC potential: the solid - with the one-body current; the dashed - with the MEC contributions for constant πNN form factors; the dash-dotted - with $F_{\pi NN}$ as indicated there.

4.4 Terra incognita

Very scanty data and theoretical models exist at energies above a few hundred MeV, or in systems with more than three nucleons. In particular, it should be very interesting to investigate if proton-neutron pairs in nuclei (quasi-deuterons bound in nuclei) exhibit the same asymmetries that we are now beginning to understand in the case of the free deuteron.

5. CIRCULARLY POLARIZED GAMMA RAYS

As we have already indicated, circularly polarized photons correspond to helicity eigenstates and therefore to definite orientations of the spin of the gamma ray, parallel or antiparallel to the direction of motion. Since the spin, like all angular momenta, is a pseudovector, the only parity-conserving observables that can be built with it are given by its scalar product with other pseudovectors, such as the spin of another particle

$$O_\sigma = \vec{s}_\gamma \cdot \vec{\sigma}_1 \qquad (4)$$

or the vector product of two momenta

$$O_P = \vec{s}_\gamma \cdot \vec{P}_1 \times \vec{P}_2 \qquad (5)$$

5.1 Spin densities

To detect the effect of O_σ we must either have a polarized target or be able to measure the spin of a particle in the final state of a photonuclear reaction. This latter type of experimentation probably requires a reaction yield and a beam intensity larger than ours, and unless some original suggestion is put forth, it now appears very difficult. On the other hand, polarized targets are available in several laboratories and the reaction of polarized gamma rays on polarized targets could be studied even today if circularly polarized photons were available.

We will summarize some points here referring to the original paper [21] for more formulas and ideas.

The differential Compton scattering cross section of circularly polarized photons on polarized electrons can be calculated with QED. It is composed of the usual unpolarized cross section and one part which depends on the direction of polarization of the electron and the photon helicity. In the electron rest frame it is given by:

$$\frac{d\sigma^{\pm}}{d\Omega} = A(k, \theta) \pm B(k, \theta, \varphi, \psi) \qquad (6)$$

where θ and φ are the polar and azimuthal angles of the photon, ψ is the polar angle of the direction of the electron spin and the $\pm$ signs refer to the two possible values of the photon helicity.

This formula can be applied to electron distributions and has been use to study spin densities in ferromagnetic materials [22]. A proposal has been advanced [23] to use the same principle to monitor the electron beam polarization in the storage ring LEP, and our set-up could be easily adapted to a study of this phenomenon at the ESRF if the information would be useful to other users.

The idea is to measure the asymmetry with respect to the photon polarization:

$$\Sigma = \frac{B}{A}\,\frac{N\uparrow - N\downarrow}{N\uparrow + N\downarrow} \qquad (7)$$

where $N\uparrow$ and $N\downarrow$ are the probabilities of finding an electron with the spin up or down.

This technique could be extended to measure any spin distribution, such as that of nucleons inside the nucleus or quarks inside the nucleon.

As an example, let us consider a model of a polarized proton composed of three free quark. In this case we must take into account not only the spin distribution of the three quarks, $q_i\uparrow$ and $q_i\downarrow$, but also their charges e_i and eq. 7 must be rewritten as:

$$\Sigma = \frac{B}{A}\,\frac{\Sigma_i\, e_i^4\,(q_i\uparrow - q_i\downarrow)}{\Sigma_i\, e_i^4\,(q_i\uparrow + q_i\downarrow)} \qquad (8)$$

We can take from reference [24]:

$$u\uparrow = 5/9,\quad u\downarrow = 1/9,\quad d\uparrow = 1/9,\quad d\downarrow = 2/9;$$

and

$$e_u = 2/3,\quad e_d = -1/3$$

which yields

$$\Sigma(\gamma p) = \frac{B}{A}\,\frac{\frac{16}{81}\left(\frac{5}{9}-\frac{1}{9}\right)+\frac{1}{81}\left(\frac{1}{9}-\frac{2}{9}\right)}{\frac{16}{81}\left(\frac{5}{9}+\frac{1}{9}\right)+\frac{1}{81}\left(\frac{1}{9}+\frac{2}{9}\right)} = \frac{B}{A}\,\frac{16\cdot 4-1}{16\cdot 6+3} = \frac{63\,B}{99\,A} = \frac{7\,B}{11\,A}$$

This is a precise prediction which can be compared with measurements made with different values of k, θ, φ, ψ and therefore the energy in the CMS, the four-momentum transfer and the ratio B/A. In this way we can perform, under various kinematical conditions, a test of the hypotheses that:

1) a nucleon is composed of three quarks;
2) under Compton scattering of polarized high-energy gamma rays the three quarks behave like free Dirac particles.

5.2 Absorption of polarized photons by polarized protons

Practically no data are available on circularly polarized photon absorption by longitudinally polarized nucleons. These very basic quantities are needed in particular to verify the Drell-Hearn-

Gerasimov sum-rule[25]. Based on a dispersion relation written for the spin dependent term of the forward Compton amplitude on the nucleon, and on the low energy theorems, this sum-rule relates the total absorption cross-section σ_p and σ_A for the respective parallel and antiparallel spin configurations to the static properties of the nucleon. It comes:

$$\int_0^\infty \frac{d\nu}{\nu} [\sigma_p(\nu) - \sigma_A(\nu)] = \frac{2\pi^2\alpha}{M_p^2} k_p^2 \approx 203\ \mu b$$

where ν is the photon energy, M the proton mass and k the anomalous magnetic moment of the proton. Since the DHG sum-rule is also connected with the EMC data on the spin proton structure function[26], this measurement will give the limit for real photons of the same quantity measured in deep inelastic scattering with virtual photons.

This experiment can be performed within a few-week period with the GRAAL beam, in connection with a polarized proton target similar to the one designed at Saclay for the Fermilab E704 experiment[27], and a large acceptance detection system for the hadronic products. Such a device was used at Saclay to measure the total photon absorption cross-section on carbon and lead in the 130-530 MeV range[28].

5.3 The three-body problem.

Circularly polarized gamma rays might provide a novel instrument for investigating a very old question: the three-body force.

It is a classical problem to understand if the force acting between two particles when they are isolated remains the same or is changed when a third particle is interacting with the two.

The observable indicated in eq.5 does not make sense if particles 1 and 2 are identical, since it is antisymmetric in their exchange:

$$O_P(1,2) = -\,O_P(2,1)$$

To overcome this difficulty we have written instead the operator:

$$O^* = \vec{s}_\gamma \cdot \vec{p}_1 \times \vec{p}_2 (E_1 - E_2)$$

which is symmetrical in the exchange of the two particles.

Since

$$\vec{s}_\gamma = \pm \hat{k}$$

then with

$$A = \hat{k} \cdot \vec{p}_1 \times \vec{p}_2 (E_1 - E_2) \qquad (9)$$

we have

$$O^* = \pm A$$

where the + signs correspond to the different values of the photon polarization.

We will now consider three different cases:

1) Two-body reactions.

For example, in the case of:

$$\gamma + d \rightarrow p + n$$

we have

$$\vec{k} = \vec{p}_p + \vec{p}_n$$

Therefore the triple product:

$$A = \hat{k} \cdot \vec{p}_p \times \vec{p}_n \equiv o$$

is identically zero since the three vectors are coplanar.

2) Quasi two-body reactions.

We consider a two-body reaction on a bound moving target:

$$\gamma + T \rightarrow p_1 + p_2$$

The conservation of energy and momentum can be written:

$$\vec{k} + \vec{p}_T = \vec{p}_1 + \vec{p}_2$$

$$k + E_T = E_1 + E_2$$

or

$$\vec{p}_2 = \vec{k} + \vec{p}_T - \vec{p}_1$$

$$E_2 = k + E_T - E_1$$

and substituting into eq. 9 we have

$$A = \hat{k} \cdot \vec{p}_1 \times (\vec{k} + \vec{p}_T - \vec{p}_1)\,(E_1 - k - E_T + E_1)$$

or

$$A = \hat{k} \cdot \vec{p}_1 \times \vec{p}_T\,(2E_1 - k - E_T) \qquad (10)$$

If in this equation we make the substitution:

$$\vec{p}_T \rightarrow -\vec{p}_T$$

then

$$E_T \rightarrow E_T$$
$$A \rightarrow -A$$

Therefore if the distribution of p_T is even:

$$n(\vec{p}_T) = n(-\vec{p}_T)$$

as in the nuclear Fermi gas model, then the distribution of A is also even:

$$N(A) = N(-A)$$

and we can see no effect by changing the polarization of the photon. If s = k is changed to s = -k then N(O*) = N(- O*).

3) A spectator plus any process.

We assume that p_1 comes from any process inside a nucleus and p_2 is the momentum of a spectator nucleon:

$$\vec{p}_2 = \vec{p}_s$$

then

$$A = \hat{k} \cdot \vec{p}_1 \times \vec{p}_s (E_1 - E_s)$$

and if

$$\vec{p}_s \rightarrow -\vec{p}_s \quad \text{then} \quad E_s \rightarrow E_s \quad \text{and} \quad A \rightarrow -A$$

and again, we can see no effect by changing the photon polarization.

Therefore we can perform an experiment, detecting two particles in the final state of a many-body photodisintegration, to measure the distribution of the quantity A or:

$$\frac{d\sigma}{dA}$$

If this distribution is not symmetric, we can measure its asymmetry free of systematic errors, by simply repeating the measurement with the photon polarization reversed.

As we have shown, simple, quasi two-body reaction mechanism cannot produce such an asymmetry. If it exists, it must be because of the contribution of more sophisticated diagrams, including three-body forces or complicated, spin-dependent, final-state interactions.

This technique might have the advantage of evidencing the effects of three-body interactions as a quantity which is different from zero only if such effects are present. A great improvement over the traditional technique of comparing the experimental data with two model calculations which differ depending on which three-body diagrams are considered.

This problem has an elegant geometrical interpretation. The direction of the photon circular polarization defines a direction of rotation in the initial states of the reaction. To make use of this information in a parity-conserving transition, we must define a direction of rotation in the final state in order to observe if the cross section has the same value whether these two directions are equal or opposite. If the spin of the particles in the final state is not observed, this definition is

provided by the vector product $\vec{p_1} \times \vec{p_2}$, with the necessary addition of $(E_1 - E_2)$ if the two particles are identical.

Let us consider the tale of two brothers who inherit two broken, still, old-fashioned watches with the two traditional arms in the same position. They part and live in different countries when, during a telephone conversation, the need arises to define a common direction of rotation.

They take the two watches and agree that the positive direction of rotation is the one which takes the small arm over the long arm with an angle of less then 180 degrees. In our case $E_1 - E_2$ tells which is the small arm, and $\vec{p_1} \times \vec{p_2}$ measures the angle of rotation.

The possible interest of O* in the detection of three-body forces can also be evidenced in a different way. O* is odd under time reversal since the time-reversal operator T changes the sign of all its three factors (s_γ to p_1 and p_2).

Therefore a simple-minded approach would suggest that its expected value is zero. However, as has been pointed out by various authors (see for example, Francis Low [29] page 24), this is true only if the system is self-adjoint. And the system is self-adjoint if it is treated in the Born approximation, but not necessarily if final-state interactions, or more complicated diagrams, are taken into account.

In conclusion, we have two different arguments suggesting that the study of asymmetry with circularly polarized gamma rays can directly evidence more sophisticated reaction mechanisms.

6. PHOTOPRODUCTION OF STRANGE PARTICLES

The possibility of obtaining high-energy gamma rays opens a new frontier in physics with flavour degrees of freedom. The (γ, K) reactions can be used to put flavour into nuclei. This will provide a precision tool to study the interactions between hyperons and nucleons. In order to gain a profound knowledge of the structure of nucleons and nuclei, it will be quite essential to learn more about the building blocks of hadrons. The photoproduction of strangeness will allow new informations on the baryon-baryon interactions

$$\gamma + d \rightarrow K^+ + (\Lambda^0 + n)$$
$$\gamma + d \rightarrow K^+ + (\Sigma^0 + n)$$
$$\gamma + d \rightarrow K^+ + (\Sigma^- + p)$$

and other few-body problems such as three-body forces

$$\gamma + He^3 \rightarrow K^+ + (\Lambda^0 + p + n)$$

charge symmetry breaking, etc.

In particular with the help of totally polarized photons, the elementary interaction

$$\gamma + p \rightarrow K^+ + \Lambda^0$$

for which little data exist, can be studied from threshold (E_γ = 912 MeV) to 1500 MeV, measuring also the transfer of polarization from the photon to the strange baryon. This is made possible by the fact that the polarization of a Λ^0 can be easily measured by the asymmetry in its decay products. Therefore it is possible to measure the correlations between the polarization of the incident gamma and that of the Λ^0 in the final state. A type of experiment that is very difficult with other recoil products such as protons and neutrons.

Another advantage of K^+ photoproduction is that in our energy range the K^+ mean-free path in nuclear matter is long compared with the dimensions of nuclei, and we can therefore investigate this process also in the nuclear core without too much distortion of the wavefunction of the outgoing K.

The total cross section for the elementary reaction:

$$\gamma + p \rightarrow K^+ + \Lambda^0$$

is of the order of 2 μb in the energy range 1-2 GeV.

Therefore with a Hydrogen target 5 cm long we have a total yield of about 2 K^+ per second:

$$n_k \approx 2\ s^{-1}$$

a comfortable rate which also allows the use of spectrometers of moderate solid angle:

$$\Delta\Omega \approx 0.1\text{-}1\ sr$$

BIBLIOGRAPHY

(1) a) Proceedings of the Workshop on Intermediate Energy Nuclear Physics with Monochromatic and Polarized Photons, Frascati, 1980, G.Matone and S.Stipcich eds., (Laboratori Nazionali di Frascati 1980);
b) Il Progetto Alfa Tre, LNF 1981;
c) Pulse Stretcher Ring, MIT-LNS 1984;
d) Nuclear Physics Research with a 450 MeV Cascade Microtron, University of Illinois 1986;
e) Research Program at CEBAF, Report of the 1986 summer study group, CEBAF, Newport News, Virginia, USA;
f) Journees d'études de physique nucléaire sur la photoproduction et l'electroproduction de mesons sur le nucleon et les noyaux, Lyon 1986;
g) Journées d'études de physique nucléaire sur la photoproduction et l'electroproduction de mesons sur le nucléon et les noyaux, Clermont-Fd 1986;
h) La physique nucleaire a courte distance, Orsay 1987;
i) Les fonctions de reponse: du nucleon.... au noyau, Grenoble 1987;
l) Workshop on heavy-quark factory and nuclear physics facility with superconducting linacs, E.De Sanctis, M.Greco, M.Piccolo and S.Tazzari eds., Courmayeur 1987.

(2) a) R.H.Milburn, Phys. Rev. Letters **10,** 75 (1963):
b) F.R.Arutyunyan and V.A.Tumanian, Phys. Letters **4**, 176 (1963).

(3) a) V.N.Bayer and V A.Khoze, Sov. J. Nuclear Phys. **2**, 238 (1969);
b) O.F.Kulikov *et al* Phys. Letters **13**, 344 (1964);
c) C.Bemporad *et al* . Phys. Rev. **138B**, 1546 (1965);
d) J.Ballam *et al.*, Phys. Rev. Letters **23**, 498 (1969).

(4) a) R.Malvano, C.Mancini and C.Schaerf: Some considerations on the possibility of obtaining a quasi-monochromatic polarized photon beam from LaseR-electron scattering in the storage ring Adone. LNF-67/48 (1967);
b) L.Casano *et al.*, Laser and Unconventional Optics Journal 55, 3 (1975);
c) G.Matone *et al.*, Lecture Notes in Physics **62**, 149 (1976): Photonuclear Reactions II, S.Costa and C.Schaerf eds. (Springer-Verlag 1977);
Invited contribution to the Europhysics Study Conf. on High Energy Laser and Scientific Applications, Oxford (1975).

(5) L.Federici *et al.*, Nuovo Cimento **59B**, 247 (1980).

(6) A.M.Sandorfi *et al.*, IEEE Trans. **NS-30**, 3083 (1983).

(7) L.Federici *et al.* Lettere al Nuovo Cimento **27**, 339 (1980).

(8) M.Preger *et al.*, Nucl. Instr. & Meth. **A249**, 299 (1986).

(9) a) ESRF: Report of the ESRP 1984;
b) ESRF Foundation Phase Report 1987.

(10) P.J.Carlos, Nuclear reactions with real photons, in ref . 1i.

(11) N.C. Mokhopadhyay *et al.* Theory of photo- and electroproduction of mesons: problems and prospects. Report of the 1985 summer study group, CEBAF.

(12) A. M. Sandorfi *et al.* Scattering of polarized photons at LEGS, BNL-42331.

(13) H.Arenhovel, Nuclear Phys. **A374**, 521 (1982).

(14) a) M.P. De Pascale *et al.* Phys. Rev. **C32**, 1830 (1985);
b) F.V. Adamian *et al.* preprint YERPHI-1061 (24) -88.

(15) H.Arenhovel, Polarized observables in deuteron photodisintegration, in ref. 1e.

(16) S.J.Brodsky and J.R.Hiller, Phys. Rev. **C28**, 475 (1983).

(17) R.Ching and C.Schaerf, Phys. Rev. **141,** 1320 (1966).

(18) F.L.Fabbri, P.Picozza and C.Schaerf, Lettere al Nuovo Cimento **3**, 63 (1972).

(19) A.A.Belyaev *et al.*, Sov.J. Nucl. Phys. **44** (2), 181 (1986).

(20) a) J.M.Laget, Three-body exchange currents: II: the ^{3}He (γ,p)d reaction, DPh-N/Saclay n° 2459 (1987);
b) V.V.Kotlyar and A.V.Shebeko, Zeitschrift fur Physik A - Atomic Nuclei **327**, 301 (1987).

(21) G.Matone et al., Physics with polarized photons, International School of Intermediate Energy Nuclear Phusics, R.Bergere, S.Costa and C.Schaerf eds. Verona 1985, (World Scientific 1986).

(22) N.Sakai et al., Phys. Rev. Letters **37**, 351 (1976).

(23) M.Placidi and R.Rossmanith, e^+ e^- polarimetry at LEP, CERN/LEP-BI/86-25 rev.

(24) F.E.Close, An Introduction to Quarks and Partons (Academic Press 1979).

(25) S.D.Drell and A.C.Hearn, Phys. Rev. Lett. **16**, 908 (1966).
S.B.Gerasimov, Soviet J. Nucl. Phys. **2**, 430 (1966).

(26) J. Ashman *et al.* Phys. Lett. B **206**, 364 (1988).

(27) P. Chaumette *et al.* DPhPE-Saclay, internal report (1988).

(28) G. Audit et al. Nuclear Physics with Electromagmetic Probes, Europhysics Conference Abstracts, p.196, Paris (1985).
L. Ghedira, These d'Etat, Orsay (1984).

(29) F.E.Low, Symmetries and Elementary Particles (Gordon and Breach 1967).